

Optical Engineering

OpticalEngineering.SPIEDigitalLibrary.org

Four-wave mixing in a ring cavity

Eugeniy E. Mikhailov
Jesse Evans
Dmitry Budker
Simon M. Rochester
Irina Novikova

Four-wave mixing in a ring cavity

Eugeniy E. Mikhailov,^{a,*} Jesse Evans,^a Dmitry Budker,^{b,c,d} Simon M. Rochester,^b and Irina Novikova^a

^aCollege of William and Mary, Department of Physics, Williamsburg, Virginia 23185, United States

^bRochester Scientific, LLC, El Cerrito, California 94530, United States

^cUniversity of California, Department of Physics, Berkeley, California 94720-7300, United States

^dJohannes Gutenberg University, Helmholtz Institute Mainz, Mainz 55099, Germany

Abstract. We investigate a four-wave-mixing process in an N interaction scheme in Rb vapor placed inside a low-finesse ring cavity. We observe strong amplification and generation of a probe signal, circulating in the cavity, in the presence of two strong optical pump fields. We study the variations in probe field gain and dispersion as functions of experimental parameters with an eye on the potential application of such a system for enhanced rotation measurements. Density-matrix calculations are performed to model the system and are shown to provide good qualitative agreement with the experiment. © 2014 Society of Photo-Optical Instrumentation Engineers (SPIE) [DOI: 10.1117/1.OE.53.10.102709]

Keywords: four-wave mixing; electromagnetically induced transparency; slow and fast light; ring resonator; Raman amplification; optical gyroscope.

Paper 140633SS received Apr. 17, 2014; revised manuscript received Jul. 9, 2014; accepted for publication Jul. 10, 2014; published online Aug. 8, 2014.

1 Introduction

Recent theoretical proposals, predicting a significant improvement in laser gyro sensitivity with the use of a “white-light” cavity,¹ have motivated a number of theoretical and experimental studies of negative dispersion in various systems.^{2–6} A promising approach relies on the manipulation of optical dispersion via coherent interactions of light with a near-resonant atomic medium. Processes such as electromagnetically induced transparency (EIT), stimulated Raman scattering (SRS), four-wave mixing (FWM), etc., are known to enable controllable group index n_g variations from subluminal (“slow light,” $n_g \gg 1$) to superluminal (“fast light,” $n_g < 1$).⁷ Demonstration of a white-light laser gyroscope requires a gain medium with a group index tunable around $n_g = 0$. Several experimental groups have pursued various approaches for the realization of such conditions.^{2,5,8–10}

Recently, our groups demonstrated that the fast-light regime with amplification can be achieved in a four-level N interaction scheme, shown in Fig. 1.^{10,11} In such a configuration, the two optical fields—the strong pump field Ω_{D1} and weak probe field α —form a regular Λ system exhibiting EIT and slow light.¹² The four-level N -scheme is completed with the introduction of the second strong pump field Ω_{D2} . A strong amplification of the probe field due to FWM is then expected if the optical transition $|4\rangle \rightarrow |1\rangle$ is allowed by the selection rules.^{13–17} At the same time, the additional Rabi splitting of the $|2\rangle$ ground state introduced by the second strong optical field Ω_{D2} provides an extra control mechanism to modify the probe field dispersion.^{18–20} Probe field propagation with no optical losses or with gain, with a smooth transition between slow- and fast-light regimes by varying the strength of one of the pump fields was theoretically demonstrated,^{10,11} making such a system an ideal testbed for explorations of the dispersion effects in a ring cavity laser for gyroscope applications.

In this work, we study the optical characteristics of the N -system (Fig. 1) and its realization in ⁸⁷Rb vapor when the weak probe field α is coupled to a low-finesse ring cavity. This is a step toward experimentally testing the concept of a white-light cavity gyroscope. We observed strong amplification of the circulating probe optical field under the FWM conditions. Moreover, even in the absence of the seeded input, an optical field at the probe frequency was generated inside the cavity in the presence of the two pump fields, with a characteristic laser threshold behavior with respect to the power of either pump. We also explored the group delay between input and output amplitude-modulated probe fields, and observed smooth tuning from positive delay (slow light) to negative delay (fast light) depending on the probe two-photon detuning.

2 Experimental Apparatus

A simplified schematic of the experimental apparatus is shown in Fig. 2. The current version of the experiment uses two external cavity diode lasers, each of which is equipped with a saturation-absorption spectroscopy frequency reference. One laser, tuned to the D_2 optical transition of ⁸⁷Rb, served as the Ω_{D2} pump field, and the second laser, operating at the ⁸⁷Rb D_1 line (795 nm), was used to generate both the Ω_{D1} pump field and the α probe optical field. For that purpose, the laser output was split by a polarizing beam splitter (PBS), and the transmitted beam was coupled into a single-mode optical fiber and phase-modulated using a fiber-coupled electro-optical modulator (fEOM) operating at the microwave frequency of 6.91468 GHz + δ_{2ph} . The power of the modulation was chosen such that the amplitude of the unmodulated carrier field was suppressed to approximately 20% of its original value, and approximately 40% of the power was transferred into each of the first modulation sidebands. The output of the fiber modulator was mode matched with the fundamental

*Address all correspondence to: Eugeniy E. Mikhailov, E-mail: eemikh@wm.edu

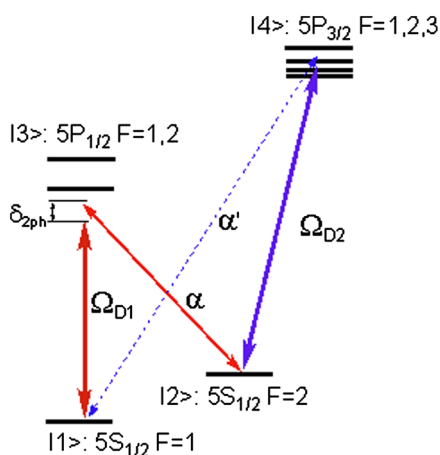


Fig. 1 A simplified N -type interaction scheme in a four-level system, and its practical realization in ^{87}Rb . The two pump fields are labeled Ω_{D1} and Ω_{D2} , the probe field α forms a Λ link with the Ω_{D1} pump field. The fourth optical field α' (not monitored in the experiment) is generated to complete the four-photon four-wave mixing (FWM) process. The two-photon detuning δ_{2ph} is the frequency difference between the $D1$ pump field Ω_{D1} and the probe field α minus the frequency of the $|2\rangle - |1\rangle$ transition.

TEM_{00} spatial mode of the ring cavity using additional lenses placed between the fiber output and the cavity input.

The direct output of the 780-nm laser (properly attenuated and linearly polarized) was used for the $D2$ pump. The laser beam at the cell is oval shaped, with minimum and maximum diameters of 2 and 3 mm, respectively. The frequency of the Ω_{D1} pump was shifted down by 80 MHz using an acousto-optical modulator with respect to the 795 nm laser output to ensure that the frequency difference between this and probe fields (α) $6.83468 \text{ GHz} + \delta_{2ph}$ was close to the ^{87}Rb ground state hyperfine splitting. This additional shift in optical frequency of the $D1$ pump helped to eliminate a parasitic interference between this field and the carrier frequency component of the fEOM output (at the original laser wavelength), which partially leaked into the ring cavity. After passing through a single-mode optical fiber, the $D1$ pump field was collimated into a Gaussian beam with a waist of 2.5 mm FWHM.

The ring cavity consisted of four flat mirrors (99.5% reflection), arranged in a square configuration, and a convex

lens (focal length 30 cm). The total length of the cavity was approximately 77 cm. One of the mirrors was mounted on a piezo-electric device (PZT), which allowed sweeping the cavity length to either observe its transmission spectrum or to lock the cavity resonance frequency to the frequency of the circulating optical field using a feedback loop.

For the current experiments, we used a cylindrical Pyrex Rb vapor cell (diameter 22 mm; length 25 mm), containing isotopically enriched ^{87}Rb and 5 torr of Ne buffer gas, placed inside a three-layer magnetic shielding to mitigate the effects of stray magnetic fields. The cell was heated to 90°C , and the value of the column density $1.2 \times 10^{12} \text{ cm}^{-2}$ was extracted by fitting the weak-probe absorption curve. The two pump fields were combined using a sharp-edge mirror at a small angle of approximately 7 mrad and entered the cavity through the input polarizing beamsplitter. Linear polarizations of both pump fields were parallel to each other, and were perpendicular to the intracavity probe field polarization. To realize the FWM configuration for the probe optical field inside the ring cavity, the two intracavity polarizing beamsplitters (PBS) were arranged such that the circulating probe field was transmitted, but the two pump fields were reflected to overlap with the probe field inside the cell, and then rejected at the second PBS. The final cavity finesse was measured to be approximately $\mathcal{F} = 18$ for light frequencies not in resonance with Rb atoms. Correspondingly, the power of the circulating probe optical field was reduced to approximately $\gamma \approx 0.70$ of its initial value after one round-trip inside the cavity:²¹

$$\mathcal{F} = \frac{\pi^4 \sqrt{\gamma}}{1 - \sqrt{\gamma}}. \quad (1)$$

The free spectral range of the cavity was measured to be 347 MHz. Since the different frequencies outputted by the EOM were not simultaneously resonant with the cavity, we were able to couple in only the probe field, while the remaining fields were reflected off the input mirror.

We used a small residual reflection of the probe optical field at the input PBS to monitor its power. To measure its spectral properties, we directed the reflected strong $D1$ pump field with a small amount of the reflected probe field into a fast photodetector, and monitored their beatnote amplitude and spectral width using a spectrum analyzer.

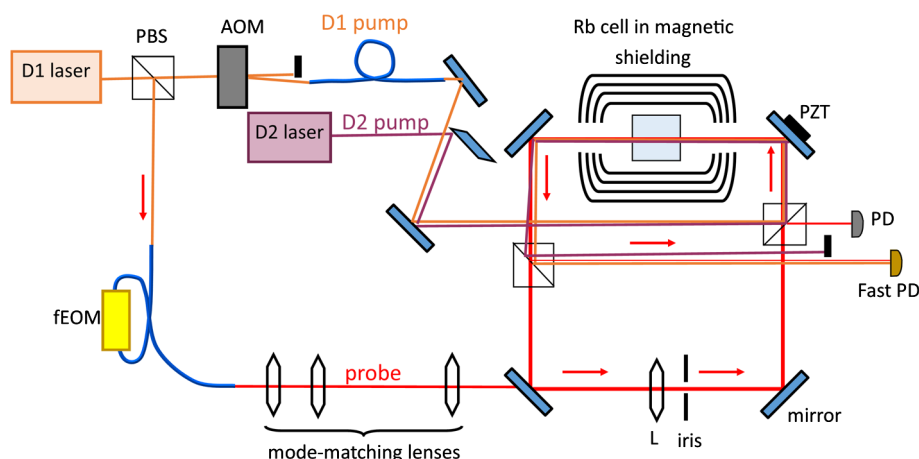


Fig. 2 A schematic of the experimental setup. See text for abbreviations.

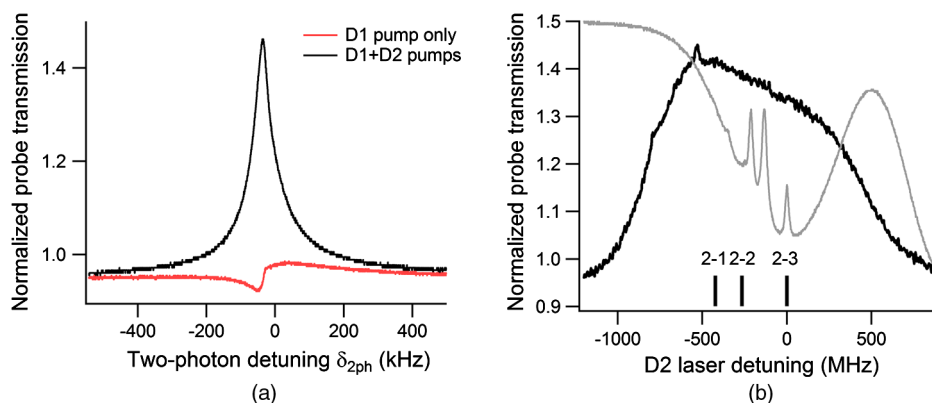


Fig. 3 (a) Examples of the single-pass probe-field transmission through the Rb cell as a function of two-photon detuning δ_{2ph} in the presence of only Ω_{D1} optical field (Λ -scheme) and of both Ω_{D1} and Ω_{D2} optical fields (N -scheme). For these measurements, the $D1$ laser is tuned ≈ 400 MHz to the red from the $5S_{1/2}F = 1 \rightarrow 5P_{1/2}F' = 1$ transition, and the $D2$ laser is tuned near the $5S_{1/2}F = 2 \rightarrow 5P_{3/2}F' = 1$ transition, (b) single-pass amplification of the probe field (black line) as a function of the $D2$ laser optical detuning (zero detuning corresponds to the $F = 2 \rightarrow F' = 3$ transition). The $D1$ laser detuning is the same as in (a), and the two-photon detuning is zero. The saturation-absorption spectrum of a reference cell (gray line), as well as the positions of $5S_{1/2}F = 2 \rightarrow 5P_{3/2}F'$ resonances are also shown. The powers of the $D1$ and $D2$ pump lasers are 0.7 and 5.4 mW correspondingly.

3 Experimental Measurements of the Probe Field Amplification and Generation

Before placing the atomic medium in the ring cavity, we confirmed single-pass amplification for the probe field in our realization of the N -interaction scheme. If only the $D1$ pump field was present, completing a single Λ link, we observed a typical two-photon Raman resonance in the probe transmission, shown in Fig. 3(a). For this measurement, we tuned the $D1$ laser to the slope of the Doppler-broadened optical transition, approximately 400 MHz to the blue from $5S_{1/2}F = 1 \rightarrow 5P_{1/2}F' = 2$ transition, to match the experimental conditions in which we later observed maximum FWM gain. Because of this relatively large one-photon detuning, the shape of the two-photon resonance was asymmetric.²² We have maintained this detuning value of the $D1$ laser from the optical transition frequency for all reported measurements. Detailed optimization of FWM at various

experimental parameters (such as optical field detunings and atomic density) will be a subject of further studies.

In the presence of the second pump field, completing the N -scheme, the probe field exhibited a strong symmetric amplification peak, with a maximum gain of ≈ 1.5 . We also measured the variation of the probe gain with the $D2$ laser detuning, as shown in Fig. 3(b). While amplification was observed in a relatively wide range of the $D2$ laser frequencies, the highest gain occurred around $5S_{1/2}F = 2 \rightarrow 5P_{3/2}F' = 1,2$ transitions, for which the selection rules allow the FWM process.

We observed even stronger amplification when the probe field circulated inside the ring cavity. Figure 4(a) shows an eight-fold increase in the probe field output when both pump fields were tuned to the FWM gain conditions. While we expect such amplification to be accompanied by the generation of the fourth optical field α' on the $|4\rangle \rightarrow |1\rangle$ optical

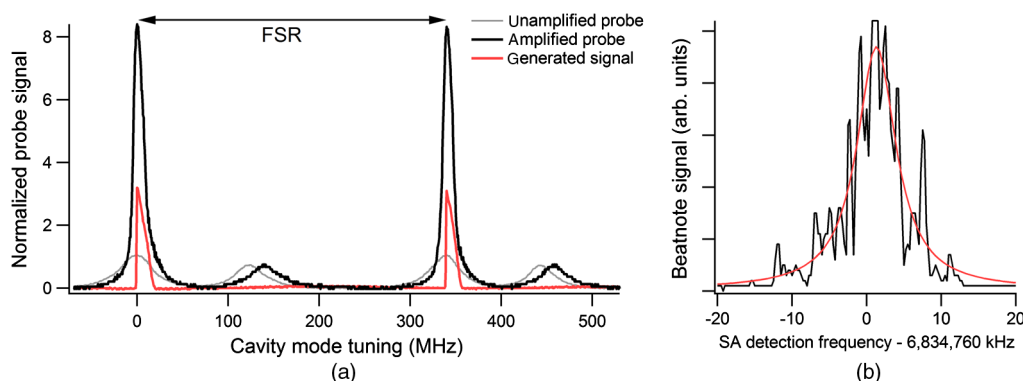


Fig. 4 (a) Cavity transmission for seeded input probe field with amplification (both pump fields are on) and without amplification ($D1$ pump is off), as well as spontaneous generation of the probe field (no probe seeding, both pumps are on). The additional smaller peaks are the off-resonant “+1” fEOM modulation sideband (the carrier field is completely absorbed), (b) the spectrum of a beatnote between the generated probe field and the $D1$ pump field. Both resolution and video bandwidth of the spectrum analyzer were set on 1 kHz. The $D1$ laser is tuned ≈ 400 MHz to the red from the $5S_{1/2}F = 1 \rightarrow 5P_{1/2}F' = 1$ transition, the $D2$ laser is tuned near the $5S_{1/2}F = 2 \rightarrow 5P_{3/2}F' = 2$ transition, and the two-photon detuning is -30 kHz. The powers of the $D1$ and $D2$ pump lasers are 0.7 and 5.4 mW, respectively.

transition (as we observed in previous studies¹¹), we were not able to directly detect it here, as the experimental arrangement did not favor its amplification. Indeed, this field has to propagate along the $D2$ pump field to satisfy the phase-matching conditions, and thus it could not circulate inside the ring cavity due to the misalignment of the $D2$ pump field from the probe intracavity direction.

When the input probe field was blocked, and only the two pump fields interacted with the atoms, we observed the generation of an optical field at the probe frequency, circulating inside the cavity. The analysis of the beatnote between this new generated field and the $D1$ pump field indicated that these two fields were phase-coherent. An example of such a beatnote spectrum, shown in Fig. 4(b), gives a rough width estimate of 6 kHz (FWHM), determined predominantly by the acoustic instabilities of the cavity. The instantaneous width appeared to be limited only by the spectrum-analyzer resolution.

The amplitude of the generated field displayed a typical threshold behavior as a function of the power of either pump beam, as shown in Fig. 5. The values of the thresholds also depended on the laser detunings and relative alignment of the pump fields. The fundamental cavity mode had, unsurprisingly, the lowest threshold values, since the pump laser parameters were optimized to maximize the gain in that mode when using the seeded probe field. However, at higher pump powers, other spatial modes were generated as well. The threshold values for those modes were at least twice as high as that for the fundamental mode, but, in general, their amplitudes were strongly affected by the cavity alignment and pump laser detunings. After the initial fast increase of the generated field amplitude above the threshold, we observed a clear saturation, for which a further increase in $D2$ laser power did not produce significant growth in the probe field power.

4 Density-Matrix Simulation of the Probe Field Propagation

A density-matrix calculation was performed to model the propagation of the pump and probe fields through the atomic medium, both for the case of a single-pass interaction, and the case in which the medium is placed in a ring cavity. The interactions of Rb atoms with the optical fields were modeled as a simplified four-level system as shown in Fig. 1. In analogy to the Rb system, we refer to the pump fields as the $D1$ and $D2$ pumps, even though the intensities and detunings of

these fields were adjusted to account for the differences between a full ⁸⁷Rb level structure and the simplified model system. (A more sophisticated calculation including the full hyperfine structure of Rb, which will allow optimization of the experimental setup, will be performed as part of future work.)

The evolution of the model four-level N -system can be described under the rotating-wave approximation by the following Hamiltonian:¹⁰

$$\hat{H} = \hbar \begin{pmatrix} 0 & 0 & -\frac{1}{2}\Omega_{D1}^* & -\frac{1}{2}\Omega_{\alpha'}^* \\ 0 & \delta_{\alpha} - \delta_{D1} & -\frac{1}{2}\Omega_{\alpha}^* & -\frac{1}{2}\Omega_{D2}^* \\ -\frac{1}{2}\Omega_{D1} & -\frac{1}{2}\Omega_{\alpha} & -\delta_{D1} & 0 \\ -\frac{1}{2}\Omega_{\alpha'} & -\frac{1}{2}\Omega_{D2} & 0 & -\delta_{\alpha'} \end{pmatrix}, \quad (2)$$

where δ_{D1} , δ_{D2} , δ_{α} , $\delta_{\alpha'}$ and Ω_{D1} , Ω_{D2} , Ω_{α} , $\Omega_{\alpha'}$ are the detunings and complex Rabi frequencies of the four optical fields, respectively, and we assume the four-photon resonance condition $\delta_{D1} - \delta_{\alpha} + \delta_{D2} - \delta_{\alpha'} = 0$, as well as the phase-matching condition on the optical wavenumbers $k_{D1} - k_{\alpha} + k_{D2} - k_{\alpha'} = 0$.

The semiclassical density-matrix evolution equations below were obtained taking into account the interaction of atoms with all optical fields, the spontaneous decay of the upper states ($|3\rangle$ and $|4\rangle$), the transit relaxation of all states due to the finite interaction time of a moving atom with the laser beams, and pressure broadening. In order to take Doppler broadening into account, the longitudinal velocity distribution was divided into velocity groups, with a set of evolution equations written for each velocity group. The equations for the rotating-frame density-matrix elements $\rho_{ab}(t, z, v)$, each a function of time t , position z , and longitudinal velocity v , are given by

$$\begin{aligned} \frac{\partial \rho_{11}}{\partial t} = & \frac{1}{2}i\rho_{31}\Omega_{D1}^* + \frac{1}{2}i\rho_{41}\Omega_{\alpha'}^* - \frac{1}{2}i\rho_{13}\Omega_{D1} - \rho_{11}\gamma_t \\ & - \frac{1}{2}i\rho_{14}\Omega_{\alpha'} + \frac{1}{2}\Gamma_3\rho_{33} + \frac{1}{2}\Gamma_4\rho_{44} + \frac{\gamma_t}{2}, \end{aligned} \quad (3)$$

$$\begin{aligned} \frac{\partial \rho_{12}}{\partial t} = & \frac{1}{2}i\rho_{32}\Omega_{D1}^* + \frac{1}{2}i\rho_{42}\Omega_{\alpha'}^* - \rho_{12}(-i\delta_{\alpha} + i\delta_{D1} + \gamma_t) \\ & - \frac{1}{2}i\rho_{14}\Omega_{D2} - \frac{1}{2}i\Omega_{\alpha}\rho_{13}, \end{aligned} \quad (4)$$

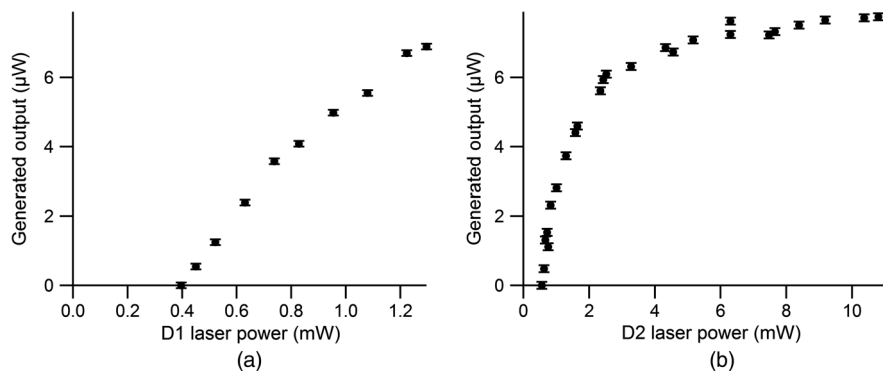


Fig. 5 The generated probe power as a function of (a) $D1$ laser power ($D2$ power maintained at 5.4 mW) and of (b) $D2$ laser power ($D1$ power maintained at 1.3 mW). The laser detunings are the same as in Fig. 4.

$$\begin{aligned} \frac{\partial \rho_{13}}{\partial t} = & -\frac{1}{2}i\rho_{11}\Omega_{D1}^* + \frac{1}{2}i\rho_{33}\Omega_{D1}^* - \frac{1}{2}i\rho_{12}\Omega_{\alpha}^* + \frac{1}{2}i\rho_{43}\Omega_{\alpha}^* \\ & - \rho_{13}\left(\frac{\Gamma_3}{2} + i\delta_{D1} + \Gamma_p + \gamma_t\right), \end{aligned} \quad (5)$$

$$\begin{aligned} \frac{\partial \rho_{14}}{\partial t} = & \frac{1}{2}i\rho_{34}\Omega_{D1}^* - \frac{1}{2}i\rho_{12}\Omega_{D2}^* - \frac{1}{2}i\rho_{11}\Omega_{\alpha'}^* + \frac{1}{2}i\rho_{44}\Omega_{\alpha'}^* \\ & - \rho_{14}\left(i\delta_{\alpha'} + \frac{\Gamma_4}{2} + \Gamma_p + \gamma_t\right), \end{aligned} \quad (6)$$

$$\begin{aligned} \frac{\partial \rho_{22}}{\partial t} = & \frac{1}{2}i\rho_{42}\Omega_{D2}^* + \frac{1}{2}i\rho_{32}\Omega_{\alpha}^* - \frac{1}{2}i\rho_{24}\Omega_{D2} - \rho_{22}\gamma_t \\ & - \frac{1}{2}i\Omega_{\alpha}\rho_{23} + \frac{1}{2}\Gamma_3\rho_{33} + \frac{1}{2}\Gamma_4\rho_{44} + \frac{\gamma_t}{2}, \end{aligned} \quad (7)$$

$$\begin{aligned} \frac{\partial \rho_{23}}{\partial t} = & -\frac{1}{2}i\rho_{21}\Omega_{D1}^* + \frac{1}{2}i\rho_{43}\Omega_{D2}^* - \frac{1}{2}i\rho_{22}\Omega_{\alpha}^* + \frac{1}{2}i\rho_{33}\Omega_{\alpha}^* \\ & - \rho_{23}\left(i\delta_{\alpha} + \frac{\Gamma_3}{2} + \Gamma_p + \gamma_t\right), \end{aligned} \quad (8)$$

$$\begin{aligned} \frac{\partial \rho_{24}}{\partial t} = & -\frac{1}{2}i\rho_{22}\Omega_{D2}^* + \frac{1}{2}i\rho_{44}\Omega_{D2}^* - \frac{1}{2}i\rho_{21}\Omega_{\alpha'}^* + \frac{1}{2}i\rho_{34}\Omega_{\alpha'}^* \\ & - \rho_{24}\left(\frac{\Gamma_4}{2} + i\delta_{D2} + \Gamma_p + \gamma_t\right), \end{aligned} \quad (9)$$

$$\begin{aligned} \frac{\partial \rho_{33}}{\partial t} = & -\frac{1}{2}i\rho_{31}\Omega_{D1}^* - \frac{1}{2}i\rho_{32}\Omega_{\alpha}^* + \frac{1}{2}i\rho_{13}\Omega_{D1} + \frac{1}{2}i\Omega_{\alpha}\rho_{23} \\ & - \rho_{33}(\Gamma_3 + \gamma_t), \end{aligned} \quad (10)$$

$$\begin{aligned} \frac{\partial \rho_{34}}{\partial t} = & -\frac{1}{2}i\rho_{32}\Omega_{D2}^* - \frac{1}{2}i\rho_{31}\Omega_{\alpha'}^* + \frac{1}{2}i\rho_{14}\Omega_{D1} \\ & - \rho_{34}\left(-i\delta_{\alpha} + \frac{\Gamma_3}{2} + \frac{\Gamma_4}{2} + i\delta_{D2} + \gamma_t\right) + \frac{1}{2}i\Omega_{\alpha}\rho_{24}, \end{aligned} \quad (11)$$

$$\begin{aligned} \frac{\partial \rho_{44}}{\partial t} = & -\frac{1}{2}i\rho_{42}\Omega_{D2}^* - \frac{1}{2}i\rho_{41}\Omega_{\alpha'}^* + \frac{1}{2}i\rho_{24}\Omega_{D2} \\ & + \frac{1}{2}i\rho_{14}\Omega_{\alpha'} - \rho_{44}(\Gamma_4 + \gamma_t), \end{aligned} \quad (12)$$

$$\begin{aligned} \rho_{21} = \rho_{12}^*, \rho_{31} = \rho_{13}^*, \rho_{32} = \rho_{23}^*, \rho_{41} = \rho_{14}^*, \\ \rho_{42} = \rho_{24}^*, \rho_{43} = \rho_{34}^*, \end{aligned} \quad (13)$$

where Γ_3 and Γ_4 are the decay widths of the upper states, Γ_p is the pressure broadening of the excited states, and γ_t is the atom transit rate through the laser beam.

These equations are coupled to the one-dimensional wave equations for the four optical fields, with the coupling for a particular optical frequency proportional to the total atomic

polarization at that frequency, obtained by summing over all velocity groups. The wave equations are given by

$$\frac{\partial \Omega_{D1}}{\partial z} + \frac{1}{c} \frac{\partial \Omega_{D1}}{\partial t} = i \frac{3\lambda_{D1}^2 \Gamma_3}{4\pi} \sum_v n_v \rho_{31}(t, z, v), \quad (14)$$

$$\frac{\partial \Omega_{\alpha}}{\partial z} + \frac{1}{c} \frac{\partial \Omega_{\alpha}}{\partial t} = i \frac{3\lambda_{\alpha}^2 \Gamma_3}{4\pi} \sum_v n_v \rho_{32}(t, z, v), \quad (15)$$

$$\frac{\partial \Omega_{D2}}{\partial z} + \frac{1}{c} \frac{\partial \Omega_{D2}}{\partial t} = i \frac{3\lambda_{D2}^2 \Gamma_4}{4\pi} \sum_v n_v \rho_{42}(t, z, v), \quad (16)$$

$$\frac{\partial \Omega_{\alpha'}}{\partial z} + \frac{1}{c} \frac{\partial \Omega_{\alpha'}}{\partial t} = i \frac{3\lambda_{\alpha'}^2 \Gamma_4}{4\pi} \sum_v n_v \rho_{41}(t, z, v), \quad (17)$$

where c is the speed of light, the λ 's are the light wavelengths, and n_v is the atomic density of each velocity group according to the Maxwell–Boltzmann distribution.

In the steady state, all time derivatives were set to zero, and the equations reduced to a set of differential algebraic equations in the spatial variable that could be solved as an initial-value problem to find the change in optical fields upon a single pass through the medium. Figure 6 shows the single-pass probe gain as a function of two-photon detuning with the $D1$ pump only and with both $D1$ and $D2$ pumps, for comparison with the experimental results of Fig. 3. The following input parameters were chosen to approximately match the parameters for ^{87}Rb and the experimental setup: excited-state natural widths $\Gamma_3 = \Gamma_4 = 2\pi \times 6$ MHz, pressure broadening $\Gamma_p = 2\pi \times 50$ MHz, Doppler width 330 MHz, optical fields' wavelengths $\lambda_{D1} = \lambda_{\alpha} = 795$ and $\lambda_{D2} = \lambda_{\alpha'} = 780$ nm, and the optical path length through the atomic medium was 2.5 cm. The remaining parameters in the calculation were adjusted by hand to improve the agreement with the experimental measurements shown in Fig. 3: transit relaxation rate $\gamma_t = 2\pi \times 20$ kHz, $D1$ pump detuning $\delta_{D1} = -2\pi \times 800$ MHz, $D2$ pump detuning $\delta_{D2} = 0$ MHz, $D1$ pump intensity 3 mW/cm², $D2$ pump intensity 3 mW/cm², probe intensity 0.5 mW/cm², and atomic density 9.6×10^{10} cm⁻³ (0.2 times the experimental value; this scaling was necessary because the four-level model system has

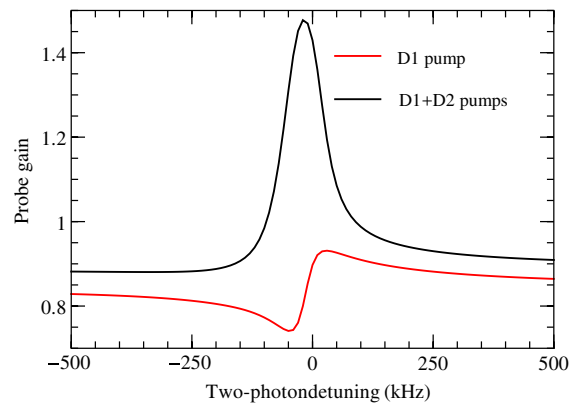


Fig. 6 Single-pass probe gain as a function of two-photon detuning in the presence of only the $D1$ pump field and both the $D1$ and $D2$ pump fields.

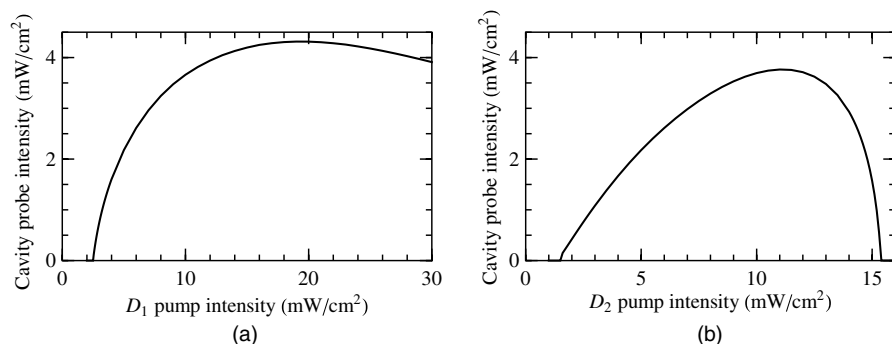


Fig. 7 Calculated generated probe intensity (inside the cavity) as a function of (a) $D1$ pump intensity and (b) $D2$ pump intensity.

intrinsically larger optical coupling constants than Rb). These values were used for all of the following results except where noted.

The propagation dynamics of the probe field inside the ring cavity were characterized by two main parameters: the single-pass complex gain through the atomic medium g_{sp} , which accounted for the effect of the interactions with the atomic medium and which was calculated according to the method described above; and the complex “gain” for one round trip of the probe light through the empty cavity g_{ec} that described all intracavity losses and the accumulated optical phase shift. (Although g_{ec} is called a “gain,” its absolute value is always less than unity.) The generated probe amplitude and frequency were numerically found by solving for the condition of stable single-mode oscillation, namely, that the total complex gain for one round-trip inside the cavity was equal to unity: $g_{sp}g_{ec} = 1$.

Figure 7 shows the circulating generated probe intensity in the cavity as a function of $D1$ and $D2$ pump intensities. The parameters are as given above, except that the $D2$ pump intensity was fixed at 6 mW/cm^2 in Fig. 7(a) and the $D1$ pump intensity was fixed at 6 mW/cm^2 in Fig. 7(b). The magnitude of the round-trip empty cavity gain $|g_{ec}| = \sqrt{\gamma} = 0.84$ was determined from the experimental finesse measurements using Eq. (1). In order to allow lasing of the probe field, the phase of g_{ec} was adjusted (corresponding to tuning the cavity resonance frequency), so that the total round-trip phase shift $\arg(g_{sp}g_{ec})$ crosses zero within the gain feature (Fig. 8).

The calculated dependences of the generated probe intensity on the intensities of each pump optical field (at the fixed

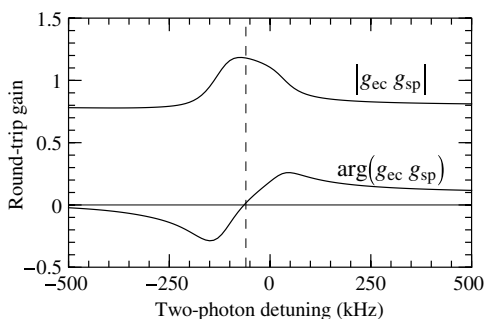


Fig. 8 Magnitude and argument of the complex round-trip gain $g_{sp}g_{ec}$. The cavity has been tuned, so that the argument crosses zero within the gain feature.

value of the other pump intensity), shown in Fig. 7, clearly demonstrate the generation thresholds followed by a rapid increase in the generated probe power, similar to the experimental observations. For higher pump powers, however, the probe intensity levels off and then falls. The beginning of this saturation was also observed in Fig. 5(b) as a function of the $D2$ pump power, while the limited available power in the $D1$ laser prevented us from reaching this regime in Fig. 5(a). However, neither laser was powerful enough to observe the reduction of the generated probe power in the limit of high powers (although such a fall-off was experimentally observed in the case of different laser detunings).

The calculation indicates that this behavior was a result of the saturation and the decrease of the single-pass gain g_{sp} as a

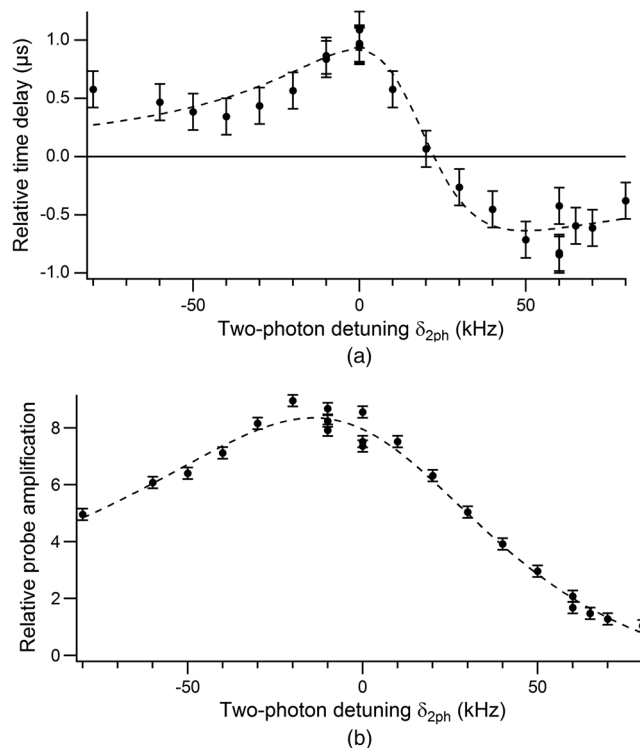


Fig. 9 Relative time difference between the output and input sinusoidal amplitude modulations in the seeded probe signal, (a) and relative amplification of the cw probe signal, (b) as functions of the two-photon detuning. The dashed lines are to guide the eye. The powers of the pump lasers are 0.4 mW ($D1$) and 4.0 mW ($D2$), and the laser detunings are the same as in Fig. 4.

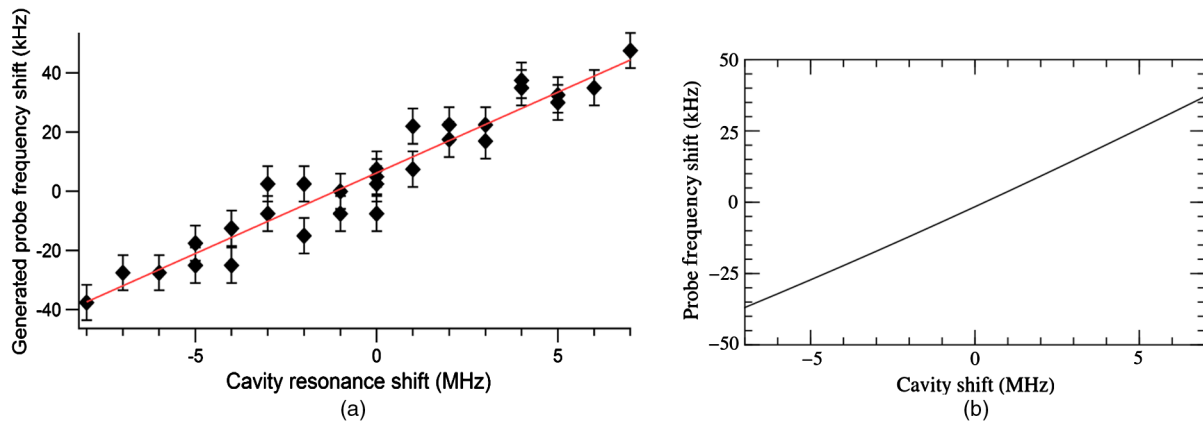


Fig. 10 (a) The change in the generated field frequency as a function of the cavity resonance tuning. The powers of the pump lasers are 0.6 mW ($D1$) and 8.2 mW ($D2$), and the laser detunings are the same as in Fig. 4, (b) corresponding numerical simulations, with $D1$ and $D2$ pump intensities both set to 6 mW/cm².

function of pump intensity. Even though the magnitude of the single-pass gain did not fall below unity, it eventually fell below the threshold needed to overcome the cavity losses and sustain lasing. The saturation effect did not occur if both of the pump intensities were simultaneously increased—the correct balance of pump intensities is evidently required for optimal probe gain in the medium.

5 Delay/Advance Measurement

Next, we evaluated the dispersive properties of the system by sending an amplitude-modulated probe field and measuring its relative time shift after the cavity. For these measurements, we actively locked the length of the cavity to a transmission resonance, and, in addition, introduced a 10% sinusoidal amplitude modulation at frequency f_{am} . We verified that with careful choice of the modulation parameters this modulation did not affect the cavity lock. For these measurements, we chose the powers of the two pump fields such that only amplification and no generation occurred in the cavity. The output probe signal maintained the sinusoidal shape, and thus we determined the relative time lag between the output and reference signals from changes in the phase fitting parameter. The reference phase was measured when both pump fields were blocked, and the probe field was far detuned from the atomic resonance. Figure 9 shows the variation of the observed time shifts as we tuned the probe two-photon detuning through the gain profile. Near the maximum, we observed a relative delay. However, for increasing positive detunings, this delay smoothly changed into advancement, indicating superluminal pulse propagation.

6 Cavity Pulling

It is important to point out that the spectral bandwidth of the FWM gain (≤ 100 kHz) was significantly narrower than the cavity transmission resonance (≈ 20 MHz), and thus our current experiment cannot be considered a realization of the original theoretical proposal.¹ Under such conditions, we expect that the frequency and the width of the probe field, generated inside a cavity, will be dominated by the spectral properties of the $D1$ laser field. However, we observed that the change in the cavity length produced a measurable effect on the generated probe frequency, as shown in Fig. 10.

For these measurements, we injected into the cavity an off-resonant “+1” modulation sideband and adjusted the

FEOM modulation frequency such that its maximum transmission occurred at the same cavity length as the probe field generation. Since this field was sufficiently weak and detuned far from any two-photon resonances, its presence in the cavity did not affect the FWM process. At the same time, locking the cavity resonance to the transmission peak of this seeded field allowed us to change the cavity length in a highly controllable manner, and observe a systematic frequency shift of the generated probe field as the cavity was swept across the transmission resonance. A numerical calculation of the cavity pulling was also performed, using the techniques described in Sec. 4, and it was in good agreement with the experimental results, as seen in Fig. 10(b). It is easy to see that in the current experimental configuration, the frequency of the generated field was only weakly affected by the cavity length variation, and was mostly determined by the narrow width of the FWM gain line. For a gyroscope implementation, it will be important to achieve a regime in which the cavity linewidth is narrower than the FWM resonance.

7 Conclusions

In conclusion, we have analyzed the propagation of a weak resonant probe through a medium of four-level atoms in an N -scheme with FWM generation allowed, and found it to be a promising candidate for the realization of tunable “slow-to-fast” light with a positive gain. This is particularly interesting for the experimental investigation of potential techniques for the enhancement of optical-gyroscope performance.

Acknowledgments

The authors thank Frank A. Narducci and Jon Davis for useful discussions, and Gleb Romanov for helping with the experiment. This research was supported by the Naval Air Warfare Center STTR program, Contract No. N68335-13-C-0227.

References

1. M. S. Shahriar et al., “Ultrahigh enhancement in absolute and relative rotation sensing using fast and slow light,” *Phys. Rev. A* **75**(5), 053807 (2007).
2. G. S. Pati et al., “Demonstration of a tunable-bandwidth white-light interferometer using anomalous dispersion in atomic vapor,” *Phys. Rev. Lett.* **99**(13), 133601 (2007).
3. G. S. Pati et al., “Demonstration of displacement-measurement-sensitivity proportional to inverse group index of intra-cavity medium in a ring resonator,” *Opt. Commun.* **281**(19), 4931–4935 (2008).

4. C. Ciminelli et al., "Fast light generation through velocity manipulation in two vertically-stacked ring resonators," *Opt. Express* **18**(3), 2973–2986 (2010).
5. M. Salit, K. Salit, and P. Bauhahn, "Prospects for enhancement of ring laser gyroscopes using gaseous media," *Opt. Express* **19**(25), 25312–25319 (2011).
6. O. Kotlicki, J. Scheuer, and M. Shahriar, "Theoretical study on Brillouin fiber laser sensor based on white light cavity," *Opt. Express* **20**(27), 28234–28248 (2012).
7. R. W. Boyd and D. J. Gauthier, "'slow' and 'fast' light," Chapter 6 in *Progress in Optics*, E. Wolf, Ed., pp. 497–530, Elsevier, North-Holland (2002).
8. H. N. Yum et al., "Superluminal ring laser for hypersensitive sensing," *Opt. Express* **18**(17), 17658–17665 (2010).
9. J. Zhang et al., "White-light cavity based on coherent raman scattering via normal modes of a coupled cavity-and-atom system," *Phys. Rev. A* **81**(3), 033804 (2010).
10. N. B. Phillips et al., "Controllable steep dispersion with gain in a four-level N -scheme with four-wave mixing," *J. Mod. Opt.* **60**(1), 64–72 (2013).
11. I. Novikova et al., "Tunable lossless slow and fast light in a four-level N -system," *Proc. SPIE* **8636**, 86360C (2013).
12. M. D. Lukin, "Colloquium: trapping and manipulating photon states in atomic ensembles," *Rev. Mod. Phys.* **75**(2), 457 (2003).
13. M. D. Lukin et al., "Quantum noise and correlations in resonantly enhanced wave mixing based on atomic coherence," *Phys. Rev. Lett.* **82**(9), 1847 (1999).
14. E. E. Mikhailov, Y. V. Rostovtsev, and G. R. Welch, "Experimental study of Stokes fields linewidth in resonant four-wave mixing in Rb vapour," *J. Mod. Opt.* **49**(14), 2535–2542 (2002).
15. N. B. Phillips, A. V. Gorshkov, and I. Novikova, "Slow light propagation and amplification via electromagnetically induced transparency and four-wave mixing in an optically dense atomic vapor," *J. Mod. Opt.* **56**(18), 1916–1925 (2009).
16. T. Hong et al., "Realization of coherent optically dense media via buffer-gas cooling," *Phys. Rev. A* **79**(1), 013806 (2009).
17. N. B. Phillips, A. V. Gorshkov, and I. Novikova, "Light storage in an optically thick atomic ensemble under conditions of electromagnetically induced transparency and four-wave mixing," *Phys. Rev. A* **83**(6), 063823 (2011).
18. R. Fleischhaker and J. Evers, "Four-wave mixing enhanced white-light cavity," *Phys. Rev. A* **78**(5), 051802 (2008).
19. T. Abi-Salloum et al., "Four-level ' N -scheme' in bare and quasi-dressed states pictures," *J. Mod. Opt.* **56**(18), 1926–1932 (2009).
20. R. T. Glasser, U. Vogl, and P. D. Lett, "Stimulated generation of superluminal light pulses via four-wave mixing," *Phys. Rev. Lett.* **108**(17), 173902 (2012).
21. A. E. Siegman, *Lasers*, University Science Books, Sausalito, CA (1986).
22. E. E. Mikhailov et al., "Large negative and positive delay of optical pulses in coherently prepared dense Rb vapor with buffer gas," *Phys. Rev. A* **69**(6), 063808 (2004).

Eugeniy E. Mikhailov is an assistant professor at the College of William and Mary. He received his BS degree in engineering physics from the Moscow State Engineering-Physics Institute (MEPhI) in 1998, and his PhD degree in physics from Texas A&M University in 2003. His current research interests include coherent light atom-interactions and their applications for quantum optics and precision metrology, quantum sensors for gravitational wave detectors. He is a member of APS.

Jesse Evans received his BS degree from the College of William and Mary in 2014. The results reported here represent a large part of his senior honors thesis.

Dmitry Budker is a co-founder of Rochester Scientific, LLC. He is the Matter-Antimatter Asymmetry Section leader at the Helmholtz Institute (Mainz, Germany), as well as a professor of physics at Berkeley.

Simon M. Rochester is a co-founder of Rochester Scientific, LLC, a scientific consulting, software development, and research company in the field of atomic, molecular, and optical (AMO) physics, focusing on resonant light-matter interactions. He received his BA degree in physics and mathematics from the University of California, Berkeley, in 1997, and his PhD degree in physics from U.C. Berkeley in 2010.

Irina Novikova is an associate professor at the College of William and Mary. She received her BS degree in engineering physics from the Moscow State Engineering-Physics Institute (MEPhI) in 1998, and her PhD degree in physics from Texas A&M University in 2003. Her current research interests include slow, fast and stored light in resonant atomic media, and quantum optics with atoms. She is a member of OSA and APS.